

CURRENT BUILDUP IN EMERGING SERPENTINE FLUX TUBES

E. PARIAT^{1,3}, S. MASSON², AND G. AULANIER²

¹ Space Weather Laboratory, NASA Goddard Space Flight Center Greenbelt, MD 20771, USA; epariat@helio.gsfc.nasa.gov

² LESIA, Observatoire de Paris, CNRS, UPMC, Université Paris Diderot, 5 place Jules Janssen, 92190 Meudon, France

Received 2009 June 9; accepted 2009 July 6; published 2009 August 6

ABSTRACT

The increase of magnetic flux in the solar atmosphere during active-region formation involves the transport of the magnetic field from the solar convection zone through the lowest layers of the solar atmosphere, through which the plasma β changes from > 1 to < 1 with altitude. The crossing of this magnetic transition zone requires the magnetic field to adopt a serpentine shape also known as the sea-serpent topology. In the frame of the resistive flux-emergence model, the rising of the magnetic flux is believed to be dynamically driven by a succession of magnetic reconnections which are commonly observed in emerging flux regions as Ellerman bombs. Using a data-driven, three-dimensional (3D) magnetohydrodynamic numerical simulation of flux emergence occurring in active region 10191 on 2002 November 16–17, we study the development of 3D electric current sheets. We show that these currents buildup along the 3D serpentine magnetic-field structure as a result of photospheric diverging horizontal line-tied motions that emulate the observed photospheric evolution. We observe that reconnection can not only develop following a pinching evolution of the serpentine field line, as usually assumed in two-dimensional geometry, but can also result from 3D shearing deformation of the magnetic structure. In addition, we report for the first time on the observation in the UV domain with the *Transition Region and Coronal Explorer (TRACE)* of extremely transient loop-like features, appearing within the emerging flux domain, which link several Ellerman bombs with one another. We argue that these loop transients can be explained as a consequence of the currents that build up along the serpentine magnetic field.

Key words: methods: numerical – MHD – Sun: magnetic fields – Sun: photosphere – Sun: UV radiation

Online-only material: mpeg animation

1. INTRODUCTION

The emergence of magnetic structures in the solar corona from the convection zone is a central process of solar physics. The intense magnetic fields that constitute active regions, sources of intense solar activity, are generated in the solar interior, and thus the magnetic flux must be transported from the solar interior into the solar atmosphere. The solar photosphere being the lowest solar layer from where electromagnetic radiation is emitted freely, extremely limited information is available below that surface. Therefore most of the efforts to understand the emergence process involve state-of-the-art numerical simulations (see the reviews by Moreno-Insertis 2007; Archontis 2008).

The crossing of the lowest layers of the solar atmosphere, photosphere and chromosphere, is particularly challenging to model. In less than 3 Mm, the main thermodynamic quantities (density, pressure, and temperature) present variations of several order of magnitudes; the plasma dynamics transit from gas pressure driven to magnetic field driven; the ionization becomes very weak; and, important radiative transfer mechanisms occur. No numerical simulations are yet able to tackle the emergence process, as three dimensional (3D), with magnetic fields of intensity and scale that would lead to the formation of active regions in a self-consistent way. Despite their limitations, recent numerical simulations (e.g., Abbett 2007; Arber et al. 2007; Archontis et al. 2004, 2009; Cheung et al. 2007, 2008; Galsgaard et al. 2007; Isobe et al. 2005, 2007; Leake & Arber 2006; Murray et al. 2006; Murray & Hood 2008; Martínez-Sykora et al. 2008) are bringing a considerable amount of new information on the

relevant physics of the emergence, and fast progress is being made.

The constantly improving observations of emerging flux regions (EFRs), driven by higher and higher spatial and temporal resolutions, also bring their share of new results (see the review by Schmieder & Pariat 2007). During its 2000 January Antarctica flight, the *Flare Genesis Experiment (FGE)*; Bernasconi et al. (2000) observed an EFR with a pixel-size resolution of 0.2 and revealed that the magnetic field is extremely fragmented in the inter-spot region with an intermittent distribution of opposite-sign polarities (Bernasconi et al. 2002). Detailed studies of the magnetic field structure, in particular using a linear force-free extrapolation, revealed that the distribution was not random and that many bipoles were linked together by undulated field lines (Bernasconi et al. 2002; Pariat et al. 2004, 2006). Pariat et al. (2004) revealed that the traditional model (Zwaan 1985) of the smooth emergence of a convex (Ω -shaped) magnetic flux tube into the solar atmosphere was incomplete: at the photosphere/chromosphere level the emerging magnetic flux tubes assume the “*sea-serpent*” geometry previously suggested by Strous et al. (1996).

This result received new confirmation by the unprecedented observations of EFR by the *Hinode*/Solar Optical Telescope (Tsuneta et al. 2008). Studying an EFR in the vicinity of AR 10926, Magara (2008) confirmed the extremely high degree of fragmentation of the field in the inter-spot region. Using spectro-imaging and spectro-metric measurements, Watanabe et al. (2008) observed a periodic distribution of the longitudinal field and of the transverse magnetic field, suggesting the presence of an undulated magnetic flux tube. Their observations agree with the suggestion of Magara (2001) and Pariat et al. (2004) that the undulations are related to the

³ College of Science, George Mason University, Fairfax, VA 22030, USA.

magnetic Rayleigh–Taylor instability (Parker 1966). Comparing the *Hinode* high-resolution observations with a realistic 3D numerical simulation of a relatively modest EFR (10^{19} Mx) at the photospheric level, Cheung et al. (2008) confirmed that the magnetic flux tubes assumed a serpentine geometry. However, carefully studying the dynamics of the emerging flux tube, they clearly demonstrated that the U-shaped segments resulted from convective downdrafts.

Given that flux tubes have a serpentine shape at the photospheric level, one must nonetheless explain how they later assume the global Ω shape of the large scale (active region) coronal loops. This undulated shape is conceptually problematic because plasma necessarily flows toward the lowest U-part of the flux tubes, anchoring them to the photosphere and therefore inhibiting their emergence. However, Pariat et al. (2004) suggested that several magnetic reconnections would allow the magnetic flux to be transferred to the upper layers of the solar atmosphere, the dense solar plasma being left at the photospheric level. This hypothesis was based on the evidence that the serpentine flux tubes were closely associated with observed localized release of energy known as Ellerman bombs (EBs).

EBs (Ellerman 1917) are typical features of the emerging magnetic flux regions (see the review by Schmieder & Pariat 2007) and consist of brief emissions that are spatially well localized and observable in the wings of chromospheric lines (Severny 1968; Kitai 1983; Fang et al. 2006; Pariat et al. 2007; Otsuji et al. 2007). Several recent studies have shown that EBs are the result of reconnection in the lower layer of the atmosphere (Georgoulis et al. 2002; Pariat et al. 2004; Fang et al. 2006; Pariat et al. 2007) as initially suggested by Rust & Keil (1992).

The link between EBs and U-shaped loops of emerging flux tubes has recently received multiple confirmations (Bernasconi et al. 2002; Pariat et al. 2004, 2007; Otsuji et al. 2007; Watanabe et al. 2008), giving credit to the resistive emergence scenario of Pariat et al. (2004). Another confirmation resulted from the 2.5D magnetohydrodynamic (MHD) simulation performed by Isobe et al. (2007), which demonstrated that reconnection at the U-loop generates a local heating that can account for the observed profile of EBs. Successive reconnections allow magnetic flux to be sequentially transferred higher and higher up.

In the frame of line-tied low- β numerical simulations, a U-loop indeed represents a preferential site for reconnection to occur (see the discussion in Section 6 about the validity of the line-tied approximation). The bottom of a U-loop rooted at the photosphere is also called a bald patch (BP; Titov et al. 1993). Field lines that go through BPs create a discontinuity of the field connectivity and are therefore separatrices (Titov et al. 1993; Longcope 2005). In 3D, BPs are organized as a finite segment at the photosphere and the associated field lines form a separatrix two-dimensional (2D) surface in the 3D domain. Based on a 2.5D analytical and numerical model, Billinghurst et al. (1993) demonstrated that current sheets could be easily formed along BP separatrices, provided that effective motions are applied at some of the footpoint of the separatrices. Symmetric and asymmetric shear perpendicular to the plane of the BP separatrices are among the most efficient ways to generate currents and eventually reconnection. As preferential current build-up sites, BPs have been associated with the formation of Sigmoids (Titov & Démoulin 1999; Archontis et al. 2009), and with impulsive events involving reconnection such as flares (Aulanier et al. 1998) and surges (Mandrini et al. 2002).

In the 2.5D simulation of Isobe et al. (2007), while there is no real line-tying, reconnection occurs above the U-shaped segments of the serpentine field line. Two consecutive Ω -shaped lobes, excited by the magnetic Rayleigh–Taylor instability, are brought into contact, and the oppositely directed magnetic fields lead to the formation of a vertical current sheet and eventually reconnect. In this model the EBs are formed by pinching motion above the U-loop of the serpentine field line (as in the cartoon of Georgoulis et al. 2002, Figure 12(a)). This evolution is essentially a 2D way to obtain reconnection at BP separatrices. A similar mechanism has also been observed at a larger scale in 3D MHD simulation (Archontis et al. 2009). In this simulation a highly twisted flux tube emerges, leading to the formation of large sigmoids. Due to the rotation of the field lines, the concave parts of the field lines form BPs at the photospheric level, in which plasma accumulates, tying the emerging flux tube to the lower layer of the atmosphere. Vertical current sheets eventually develop at the BPs, leading to reconnection and the upward transport of the magnetic flux tube in a way consistent with the scenario of Pariat et al. (2004). The 3D BP reconnection involves the interaction of neighboring highly twisted field lines above the BPs within the vertical current sheet: reconnections involve segments of unique field lines having opposite magnetic direction and the process can therefore be described in 2.5D geometry.

However, the formation of such vertical current sheets and such pinching requires converging motions in the chromosphere on both sides of U-loop/BP. If such motions exist indeed, their occurrence would have to be frequent to explain all of the EBs occurring in an emerging flux event. In Archontis et al. (2009), the pinching is a consequence of the extension of the emerging flux tube above the photosphere, whereas in Isobe et al. (2007) the pinching is the natural consequence of the growth of the lobes induced by the magnetic Rayleigh–Taylor instability, most of the other evolution being possibly inhibited by the 2.5D approximation. Are these motions very frequent in the real 3D solar chromosphere? The simulation of emergence in a realistic photosphere (Cheung et al. 2008) as well as the magnetic extrapolation of an emerging region observed with high spatial resolution (Pariat et al. 2004) reveals that, at the photospheric level, the emerging field lines tend to be relatively flat, even though they have a serpentine shape. Highly pronounced-U-shaped loop would thus not be that frequent. Finally, reconnection occurring above BPs fails to explain properly how EBs can be formed at the footpoint of the BP separatrices, as observed by Pariat et al. (2004).

The primary question that we want to answer is: how do currents build up in 3D emerging serpentine field lines? Are vertical currents frequently formed in a 3D EFR? Do currents form all along the BP separatrices, as suggested by Billinghurst et al. (1993)? In order to address these questions, we will use the set of observations and numerical simulations previously analyzed by Masson et al. (2009, hereafter MPAS09). In MPAS09, using a potential field extrapolation of AR 10191 as an initial condition, we conducted a low- β resistive MHD simulation of the observed ribbon flare that occurred on 2002 November 16. Using UV observations from the *Transition Region and Coronal Explorer* (TRACE; Handy et al. 1999) and magnetograms acquired with the *SOHO*/Michelson Doppler Imager (MDI; Scherrer et al. 1995), we noted that flux emerged prior to the C-class flare and determined that the flare was a consequence of that flux emergence. Driving the simulated system by line-tied diverging boundary motions, so as to emulate

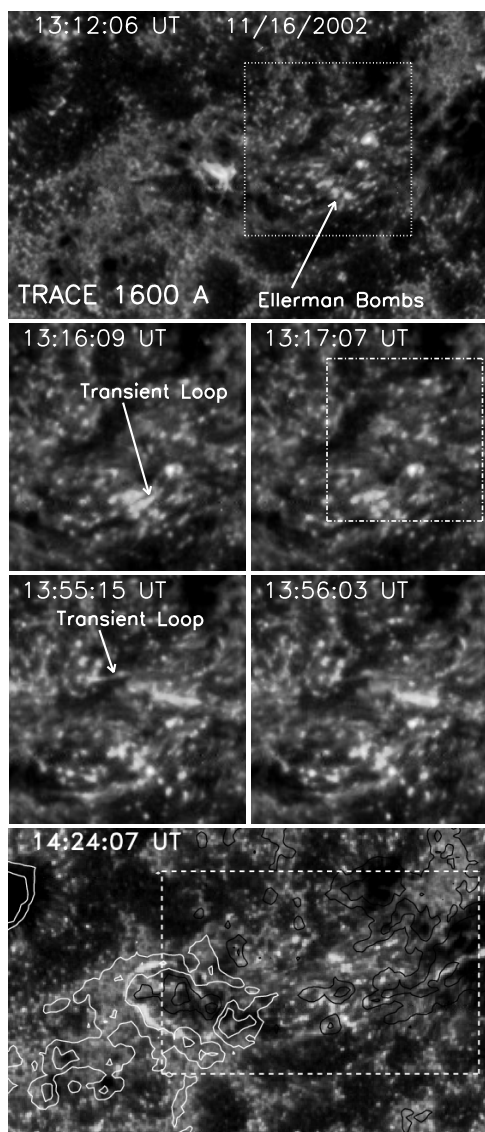


Figure 1. *TRACE* observations in the 1600 Å bandpass of the AR10191 on 2002 November 16. Top and bottom panels: general view with a field of view is $192'' \times 192'' = 141 \text{ Mm} \times 141 \text{ Mm}$. In the bottom panel, isocontours of the co-aligned longitudinal magnetic field distribution observed by MDI are drawn. The white (black) lines correspond to $b_l = [250, 600] \text{ G}$ ($b_l = [-250, -600] \text{ G}$). The dashed box represent the field of view of the lower panel of Figure 2. In the top panel the dotted rectangle present the field of view of the four middle panels. Middle panels: close-up views (field of view of $67'' \times 108'' = 49 \text{ Mm} \times 79 \text{ Mm}$) of the EFR where UV EBs and two example of transient loop are observed. The dot-dashed rectangle correspond to the field of view of Figures 3–5.

(An mpeg animation of this figure is available in the online journal.)

the observed photospheric flow pattern associated with the magnetic flux emergence, we studied the buildup of the electric currents and the reconnection responsible for the ribbon flare. In the present paper we will focus on the current buildup in the emerging flux area.

The paper is organized as follows: Section 2, we will present the *TRACE* and MDI observations of AR 10191, whereas in Section 3 we will summarize the numerical model used in MPAS09. Section 4 will present the results of the numerical simulation regarding the formation of electric currents in the emerging region. We will show that the photospheric currents are related to serpentine BP separatrixes and discuss their 3D structure. Finally, in Section 5, we will discuss the implications

for EB formation and on magnetic field emergence in general (Section 6).

2. FLUX EMERGENCE AND UV OBSERVATIONS

Active region AR 10191 was observed with *TRACE* in the 1600 Å UV continuum. The pixel size and time cadence of the observations are, respectively, $0.5''$ and 3.2 s. In MPAS09, we studied the C-class flare that occurred in AR 10191 on 2002 November 16. Figure 1 (as well as the movie available in the electronic version) presents the evolution of the UV emissions. The C-class flare started at 13:57 UT when three ribbons were formed (see Figure 1, bottom panel): a quasi-circular ribbon enclosed an elongated ribbon, while another elongated ribbon was located on the west. MPAS09 explained the flare as the consequence of a flux emergence event that occurred in the inter-spot region: the emergence of a magnetic field injected free magnetic energy and eventually destabilized the magnetic configuration (following the classical model of Heyvaerts et al. 1977).

This EFR was followed with the full-disk MDI photospheric magnetograms, for which the time cadence is 96 minutes and pixel size is $1.977''$. Longitudinal magnetograms of AR 10191 are presented in Figure 2 (right panels) at different times before the C-class flare. This active region was composed of a leading negative polarity and a trailing positive polarity in which a large parasitic negative polarity is embedded. On November 15 and 16, an important flux emergence occurred in the central region of the AR, between the main polarities (Figure 2, top right panel, within the dashed white rectangle). The evolution of the magnetic field shows the appearance of several dipoles and the diverging migration of opposite-sign polarities, typical of emerging flux events (Schmieder & Pariat 2007). In Figure 2 (right panels) we also observe that the magnetic flux distribution adopts a horseshoe pattern composed of ribbon-like concentrations of positive polarities in the north and negative polarities in the south. We noted as well that several patches of positive flux, which had previously emerged to the west of the parasitic polarity, merged with the main positive polarity spot.

In the *TRACE* UV observations, in addition to the ribbon flare, numerous brief small localized brightenings can be observed in the inter-spot region (see Figure 1; they can be more clearly identified with the movie available with the electronic version). These brightenings seem to be relatively unaffected by the ribbon flare: neither their distribution nor their evolution changes significantly during the flare. These brightenings are likely to be associated with EBs (Ellerman 1917).

Indeed, recent observations have shown a statistical correlation between EBs and bright points observed in the continuum at 1600 Å by *TRACE* (Qiu et al. 2000; Georgoulis et al. 2002; Pariat et al. 2007). Qiu et al. (2000) found that the emission profile of EBs observed in $H\alpha$ wings had a correlation larger than 50% with UV brightenings observed with *TRACE*. Using FGE data, Georgoulis et al. (2002) found a similar spatial correlation. Pariat et al. (2007) also found significant agreement between UV emissions and cospatial $H\alpha$ and Ca II emissions having a spectral profile typical of EBs. In the present observations, the UV bright point lifetime, of the order of a few minutes, is typical of EBs observed in 1600 Å continuum (Qiu et al. 2000).

Co-aligning the *TRACE* 1600 Å image at 14:04 UT and the MDI magnetogram at 14:24 UT (see Figure 1, bottom panel), we first remark that the UV bright points are located in this EFR (in the center of the dashed white rectangle). In addition, the

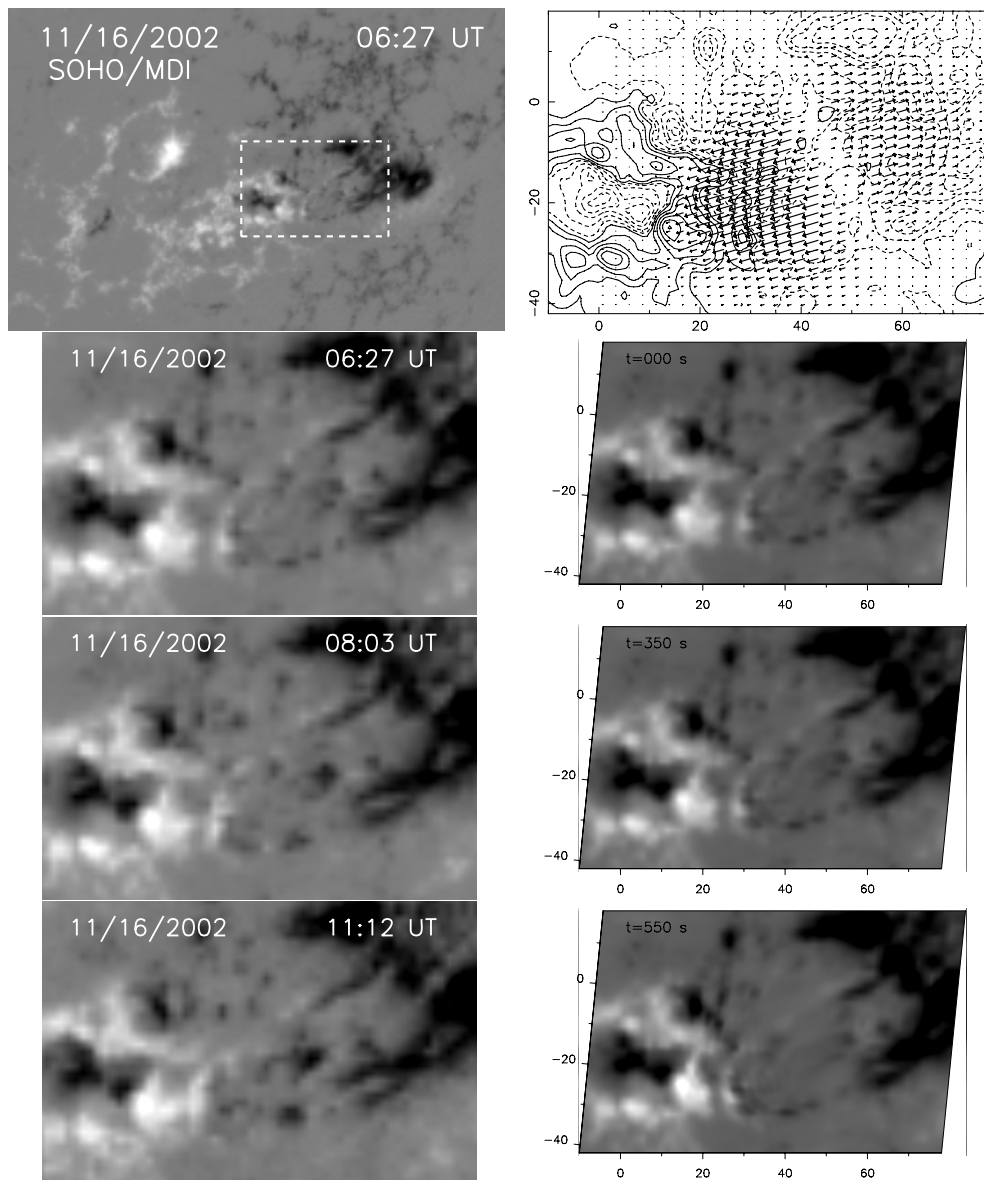


Figure 2. Right panels: MDI longitudinal magnetograms coded in shades of gray (white for positive fields and black for negative fields) at different times on 2002 November 16. The top panel has a field of view of $291 \text{ Mm} \times 189 \text{ Mm}$. The dashed box on the top panel defines the field of view (of $90 \text{ Mm} \times 60 \text{ Mm}$) of the lower left and right panels. Top right panel: photospheric flow pattern prescribed in the MHD simulation in the flux emergence area. Bottom right panels: evolution of the simulated photospheric vertical field $B_z(z=0)$. The axes x and y are in Mm.

UV brightenings tend to be located along the polarity inversion line another typical property of EBs that has been reported in numerous studies (Rust & Keil 1992; Georgoulis et al. 2002; Otsuji et al. 2007; Pariat et al. 2004, 2007; Watanabe et al. 2008). These data thus corroborate the hypothesis that the UV bright points observed at 1600 \AA are the transition-region signature of EBs.

In the vicinity of the EBs, the high-cadence *TRACE* observations also reveal the occurrence of several, very transient, elongated brightenings whose life times rarely exceed 1 minute. These loop-like structures appear in the EFR and seem to originate from the EBs. They are roughly aligned with the axis of the active region. The middle panels of Figure 1 present two examples of these transient loops (better observed in the movie available with the electronic version). In particular, the second example, occurring around 13:55 UT, seems to link regions distant of several Mm. In addition, this transient loop presents a

serpentine shape: a cusp-shaped (\wedge) section appears in its center (close to where “transient loop” is indicated in the right panel of the third row of Figure 1, the EB located at the middle of the cusp structure). Here, we are reporting these transient loop-like structures for the first time, so the question of their relationship to EBs naturally arises.

3. NUMERICAL SIMULATION

The results of the present paper are based on the same numerical simulation that was analyzed in MPAS09. The 3D visco-resistive code (Aulanier et al. 2005a; Masson et al. 2009) solves the finite- β and adiabatic MHD equations in a Cartesian box with a non-uniform fixed mesh.

The magnetic field distribution used in the simulation was given by a potential extrapolation of the MDI magnetogram taken on 2002 November 16 at 06:27 UT, several hours prior

to the ribbon flare. The use of potential extrapolations is usually a poor approximation of coronal magnetic fields and in particular those which include current carrying structures, e.g., twisted flux tubes, having a strong eruptive potential (e.g., Metcalf et al. 2008; Schrijver et al. 2008). However, unless a strong non-potential structure is present, a potential field extrapolation does not qualitatively modify the magnetic field topology (i.e., the presence of null point and BPs, which we checked by also calculating linear force-free fields). The present emerging structure being relatively small, no signature of strongly sheared structures having been observed, we believe that the potential field extrapolation is a relatively correct approximation. Furthermore, in addition to simplifying the computation, the potential field approximation allows us to start with a configuration which has zero free magnetic energy and thus enable us to follow its buildup. Therefore, even though the initial magnetic configuration is relatively unrealistic, at a latter time, after having applied some boundary evolutions, the configuration actually becomes non-potential and even non-force-free in its lowest part, as in the real solar atmosphere (Metcalf et al. 1995). The system at the time of our analysis may be a better approximation of the real field than what would result from a nonlinear force-free field extrapolation, for which important preprocessings have to be used (DeRosa et al. 2009).

Initially the plasma was assumed to be uniformly dense: $\rho = b_{\max}^2 / \mu c_{A,\max}^2 = 6.8 \times 10^{12} \text{ cm}^{-3}$, with ρ being the plasma density, b_{\max} the maximum intensity of the magnetic field \mathbf{b} , and μ the magnetic permeability. We chose the maximum of the Alfvén speed to be $c_{A,\max} = 1000 \text{ km s}^{-1}$. The initial temperature is assumed to be uniform and equal to $T = 3 \times 10^5 \text{ K}$. Even though this temperature is typically 10 times lower than in the corona, we chose this value as to obtain the best compromise to maintain initially subsonic quasi-static coronal evolution together with $\beta \ll 1$ everywhere in the low corona.

At the top and side boundaries, we assumed open conditions. At the bottom boundary, we used line-tied reflective conditions, in order to drive the corona by photospheric motions. As described in Section 2, flux emergence has occurred in the inter-spot region before the onset of the flare. We assume that this flux emergence is the driver of the flare. So as to simulate the evolution of the active region, we constrain the magnetic configuration by emulating this flux emergence event using an analytical divergent velocity field at the bottom boundary. Our numerical model is simpler than reality since we do not increase the total photospheric magnetic flux, but only simulate the observed photospheric flows. Still, the applied shearing motions lead to the injection of stress and free energy into the system, eventually leading to a substantial amount of magnetic reconnection.

Intrinsically, this approach does not fully allow us to reproduce the presence of currents in the corona. Strong electrical currents can be carried along with emerging magnetic structures (e.g., Okamoto et al. 2008; Schrijver et al. 2005), in particular during large flare events. These structures, such as twisted flux tubes, would directly inject currents in the corona. However, emerging flux simulation shows that, as flux tubes try to cross the photosphere, substantial modifications of their geometrical structure occur: the flux tubes flatten (e.g., Magara 2001; Cheung et al. 2008), and a large portion of their vertical bulk kinetic energy is transformed in important horizontal diverging and shearing motions (e.g., Magara & Longcope 2003; Archontis 2008), flows directly reproduced by our method. The

extent to which currents are formed because of direct emergence of shearing motions goes beyond the scope of this study. We believe that, to some extent, our shearing treatment of the flux emergence is nonetheless capable of capturing a large portion of the forcing processes that actually take places in the solar atmosphere and allow us to study the development of current sheets and reconnections which are necessary for the magnetic flux to rise.

The velocity field is applied to the whole area where emergence leads to separation of magnetic polarities (see MPAS09, Equations (5) and (6)). The velocity field is thus composed of a smooth gate function (to delimit the ellipsoidal/horseshoe shape of the EFR) multiplied by a sum of hyperbolic tangent functions of opposite sign (to simulate the divergence in the EFR). In order to avoid the formation of strong gradients by compressive and vortical effects at the boundaries of this region, the flow field intensity is bounded by a function formed by the product of two hyperbolic tangent functions having a weak slope. The velocity field is gradually applied, after an initial relaxation phase between $t = 0 \text{ s}$ and $t = 150 \text{ s}$, and leads to a phase with $u = \text{constant}$ for $t > 300 \text{ s}$. The maximum amplitude for the driving velocity is equal to $u_D = 20 \text{ km s}^{-1}$. Even though this value is larger than the typical observed photospheric velocities by a factor 40, it remains subsonic and largely sub-Alfvénic as required for a coronal calculation.

The prescribed velocity field, as shown in the top right panel of Figure 2, reproduces the divergence of the motion of the magnetic polarities resulting from the emergence (see Figure 2, bottom left panels). This defines a line of positive flow divergence, which is much simpler than the flows observed with MDI. Comparing the bottom right panels and the bottom left panels of Figure 2, one observes that we do not reproduce the increase of the magnetic flux present in the center of the EFR. However, the observed large-scale diverging flow pattern, i.e., the magnetic polarity separation and accumulation at both sides of the EFR, are relatively well reproduced. Thus even though, the times scale of the shearing is smaller in our simulation, its amplitude remains comparable to the one observed in the solar atmosphere. Quantifying how much stress is actually injected by our boundary motions relatively to real emergence is difficult. Our approach, while simpler, may actually introduce more field stress than a more complex full emergence. On the other hand, realistic flux emergence can also, because of the presence of an already sheared field, lead to a more dynamic evolution than what we simulate here. However, our method, by introducing differential velocities in the EFR, allows us to follow and understand qualitatively some of the characteristic process that occurs in the EFR, i.e., the intensification of current sheets.

4. 3D BALD PATCHES, CURRENT SHEETS, AND SERPENTINE FIELD LINES

At the end of the relaxation phase, at $t = 150 \text{ s}$, the bulk of the initial residual forces, resulting from the fact that the initial configuration was slightly out of numerical equilibrium, have disappeared. Nevertheless some residual currents remain, located at the boundaries. The large-scale homogeneous divergent velocity field introduced at the lower boundary induces a perturbation of the magnetic configuration in the active region, in which electric current sheets develop along various topological features. The following analysis is done at $t = 500 \text{ s}$ when driving motions have lead to substantial current intensification.

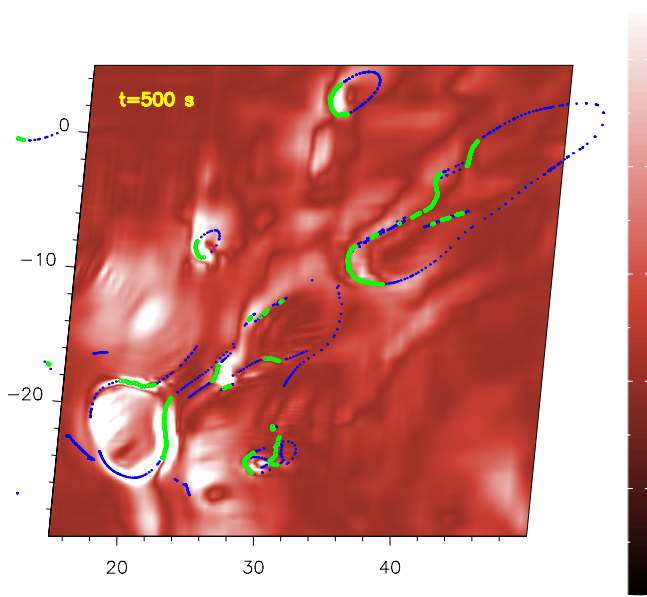


Figure 3. Bald patches (bold green dots) and the related photospheric footpoints of the separatrix field lines going through these bald patches (blue dots) in the emerging flux area at $t = 500$ s, overplotted on the total electric current $j_z(z = 0)$ coded in different shades of red (white corresponding to the most intense currents). The axes x and y are in Mm.

4.1. Photospheric Bald-patch Current Sheets

Intense current sheets develop where the driving motions have been applied, in the EFR. Figure 3 displays the location of these current sheets at the bottom boundary of the simulation domain at $t = 500$ s. Comparing the location of these sheets with the distribution of the magnetic field and its topology, we observe that the currents are not distributed randomly.

We first noticed that some of the more intense current sheets are cospatial with small-scale closed neutral lines in the photosphere. We determined the location of the BPs (Titov et al. 1993), where the field lines are concave upward (U-shaped). A BP is present when the magnetic field satisfies $\mathbf{b} \cdot \nabla b_z > 0$ at an inversion line ($b_z(z = 0) = 0$) of the photospheric/bottom boundary. The distribution of some BPs is represented with green dots in Figure 3. Finally, we integrated the field lines passing through these BPs and determined the location of their footpoints, i.e., the intersection of the BP separatrix field lines with the bottom plane. The separatrix footpoints are represented by blue dots in Figure 3. Since BPs are organized as continuous segments, the associated separatrices surface map continuous segments at their footpoints. Since we only plot a discrete finite number of BPs, a finite number of separatrix footpoints is represented and the mapping of the separatrices may appear discontinuous. Note also that not all the BP segments and separatrix footpoints within the area represented in Figure 3 have been plotted. Some minor BP regions have been left out, and some separatrix footpoints originating from BPs out of the field of view are also omitted. A few high-current regions are not associated with any topological features. Some of them are due to BPs and separatrices not shown in this figure. Some others are probably created by other topological features such as QSLs or are the wide trace of volume currents formed by the overall imposed shearing in the emerging region.

BPs are well known preferential sites for the formation of current sheets when photospheric motions are applied (Low & Wolfson 1988; Vekstein et al. 1991) in the frame of

line-tying approximation (the relevance of this approximation is discussed in Section 6). In the present simulation, most of the BPs and the BP-separatrix footpoints are cospatial with intense currents (see Figure 3). This result is in agreement with past 2.5D MHD simulations of current sheet formation in BP separatrices due to line-tied boundary motions (Billinghurst et al. 1993). In the present paper we extend their result in 3D: we observe that the horizontal distribution of the currents matches the shape of the BP separatrices. This is particularly obvious for the separatrix located at the lower left corner which presents the same \sim and \simeq shaped distributions of the current.

In Figure 3, we also note that some BPs and separatrix footpoints are not necessarily associated with intense currents. In addition, the intensity of the currents varies a lot from one topological structure to another. A first reason is related to a numerical bias. The grid has a non-uniform mesh adapted to our earlier study of a coronal null point (MPAS09). The grid spacing is smallest at the null point located at $x \simeq 12$ Mm, $y \simeq -18$ Mm and decreases geometrically from there. The resolution is thus higher in the bottom left corner of Figure 3 than in the top right one. The electric currents, derived from the curl of the magnetic field, are thus likely to be higher where the mesh size is smaller (for the current sheets which are not fully resolved in the numerical simulation). Indeed for a given magnetic field difference between the two sides of a separatrix surface, a smaller grid results in a higher magnetic field gradient. This numerical effect cannot solely explain the different intensities of the currents formed at different BPs. The currents corresponding to the BP located around $(x = 33$ Mm, $y = 2$ Mm) are relatively intense even though the resolution is relatively small. In fact, topological structures such as BP separatrices only define preferential sites for the development of intense current sheets. Other factors are necessary to increase the currents, such as the intensity of the gradients of the magnetic field.

In fact, shearing motions allow us to build up intense currents efficiently. The BPs located around $(x = 41$ Mm, $y = 1$ Mm) exhibit very low currents, because they are located where the imposed boundary shearing motions are extremely weak (see Figure 2). On the other hand, the BPs located at $(x = 20$ Mm, $y = -20$ Mm) are located in the core of the shearing pattern and are also associated with very intense current sheets. Even with similar intensity, not every motion can lead to the development of strong currents. As Billinghurst et al. (1993) showed in 2.5D, motions perpendicular to the plane of the separatrix field line are much more efficient than motion within that plane. The location of the shearing (at the BP itself versus at the BP-separatrix footpoints) influences also the intensity of the current that can be formed along the separatrix, as well as the distribution of the current formed along the field line. In any case, efficient shearing motions are essential to obtain intense electric currents along the separatrices. The specific distribution of the electric currents in a region with numerous BPs will depend both on the relative distribution of the topological magnetic structure and the driving velocity field (in the frame of smooth gradients of the velocity field).

4.2. Serpentine Field Lines

The distribution of BPs also presents another important characteristic: several groups of BPs seem to be aligned. This feature has already been noted in the EFR (Pariat et al. 2004) and is the result of an organized distribution of the magnetic field. The associated underlying photospheric magnetic field distribution

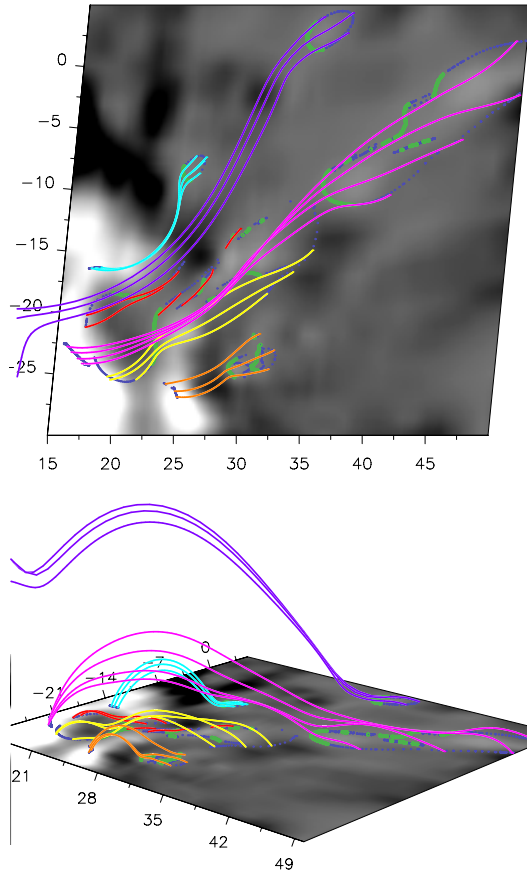


Figure 4. Line of sight view (top panel) and perspective view (bottom panel) of different groups of separatrix undulated field lines, at $t = 500$ s, plotted over the distribution of the photospheric vertical field $b_z(z = 0)$ (coded in different shades of gray, white for positive b_z and black for negative). Bald patch regions are plotted as bold green dots. The photospheric footpoints of the separatrix field lines going through these bald patches are plotted as blue dots. All of the different field lines are separatrix field lines passing through at least one bald patch. In the vertical direction a homothetic factor of 2.16 has been used to plot the field lines. The field of view is the same as in Figures 3. The axes x and y are in Mm.

presents a sequence of positive and negative polarities (Figure 4, top panel). Pariat et al. (2004, 2006) showed that in the EFR, several separatrices were passing through multiple BPs and dips (U-shaped segment, above the photosphere) and thus assumed an undulated shape. These “sea-serpents” are typical of emerging active regions (Strous et al. 1996; Pariat et al. 2004; Watanabe et al. 2008).

A similar geometry is also observed in the present simulation (see Figure 4). Note that for each BP segment, we only plot a few representative field lines. For each BP segments, these field lines are particular field lines which form the separatrix surface. The overall shape of the separatrix field lines at $t = 500$ s reveals the occurrence of several spatial undulations along their length: the yellow lines go through two U-shaped sections and some of the pink field lines go through up to four BPs and dips. The extrapolation of the magnetic field measured in the inter-spot region of an emerging active region revealed that up to five BPs dips could be linked by a single field line (Pariat et al. 2004, 2006). The numerical simulation of Cheung et al. (2008) also showed the formation of serpentine field lines having an average of five undulations (determined from a magnetic flux analysis).

Another feature present in the simulation, which had already been observed by Pariat et al. (2004), is the organized hierarchical stratification of the serpentine field lines. Small undulated

separatrices lie below larger Ω -shaped portions of other serpentine field lines. For example, the yellow lines are located below the eastern portion of the pink lines, and the cyan separatrices are below the purple field lines. Pariat et al. (2004) associated this organization with the temporal evolution of the emerging flux. The different sets of field lines represent different stages of the emergence process: the smallest lines, closest to the photosphere, correspond to the first stage of the emergence; as they further emerge, these lines become larger and reach greater heights, under which new emerging flux appears.

We note that most of the BPs and the serpentine field lines were already present at the beginning of the simulation: the distribution of the magnetic field responsible for the BPs, i.e., the alternating of positive and negative field patches was already present initially and was only slightly affected by the prescribed motions (see Figure 2). The serpentine topology is the direct consequence of the magnetic flux distribution in the observed EFR, within the approximation of the potential field approximation. However, the applied boundary motions induce the formation of 3D current sheets along these associated separatrices.

4.3. Serpentine Current Sheets

The serpentine field lines presented in Figure 4, as separatrices, define preferential sites for the formation of currents, not only at the location of the BPs, but all over their length. What is the precise distribution of the currents within these serpentine field lines?

The 3D electric current distribution at $t = 500$ s is presented in Figure 5. The top panel presents the distribution of the dimensionless index \tilde{J} :

$$\tilde{J}(x, y) = \int_{z=0}^{z_{\text{top}}} \frac{|\mathbf{j}(x, y, z)|}{|\mathbf{b}(x, y, z)|} dz \quad (1)$$

with $z_{\text{top}} = 3$ Mm. By using $|\mathbf{j}|/|\mathbf{b}|$, homogeneous to the inverse of a length, we reduce the influence of the lower resolution at the top right corner of the domain. It enhances the locations where the thin current sheets associated with separatrix form relatively to the extended volume currents. In the plotted domain there is no location of very low $|\mathbf{b}|$ and thus high \tilde{J} are mostly related to high $|\mathbf{j}|$. The vertical integration of the current distribution over the lowest layers of the solar atmosphere allows us to determine the accumulated distribution of the electric currents. It can also be used as a proxy for the electromagnetic emission originating from these part of the atmosphere.

Most of the structures in the photospheric field distribution, presented in Figure 3, are present in Figure 5, such as the \sim and \sphericalcap features located around $(x, y) = (20 \text{ Mm}, -20 \text{ Mm})$ and $(28 \text{ Mm}, -14 \text{ Mm})$. However, the most intense patches of \tilde{J} do not necessarily correspond with the largest values of photospheric currents $|\mathbf{j}|(z = 0)$. While the structure located at $(24 \text{ Mm}, -8 \text{ Mm})$ is present in both figures, the features located at $(30 \text{ Mm}, -2 \text{ Mm})$ and $(38 \text{ Mm}, -13 \text{ Mm})$ only stand out in the \tilde{J} distribution.

The reason is that intense currents build up not only at the BPs themselves but all along the separatrices surfaces, as predicted theoretically. This is illustrated in the bottom panels of Figure 5, which presents four vertical 2D cuts through the $|\mathbf{j}|/|\mathbf{b}|$ distribution. The most prominent characteristic of these cuts is the particular topology that the electric current distribution follows. Similarly to BP field lines, we clearly observe that currents have been enhanced along sheets which assume a

serpentine geometry. The cut labeled “A” indeed shows several vertical undulations of the current sheet distribution. These currents exactly follow the yellow field lines (cf. Figure 4 and Section 4.2) and the west (right) section of the pink field lines.

The hierarchical stratification of the serpentine field lines has also a counterpart in the current distribution. In the “B” and “C” cuts, the low-height electric currents located at $x \sim 20$ Mm, which can be associated with the red field lines in Figure 4, are located beneath a higher, weaker sheet of current which corresponds to the east (left) part of the pink field lines.

Because the serpentine field lines plotted in Figure 4 are not completely planar, it is not possible to follow them using 2D cuts. However, the extremely good match between some sections of these field lines and the location of thin current sheet allows us to reasonably argue that currents build up not only at the BP but all along the separatrix surfaces. We also observe that the most intense currents are localized around the Bald Patches and that, in general, the separatrices currents are a few times weaker. This confirmation of the theoretical prediction that thin current sheets form along the emerging serpentine separatrices implies several consequence for the dynamics of the EFR, as we detail in the next section.

5. TRANSIENT UV EMISSION DURING FLUX EMERGENCE

TRACE observations in the 1600 Å bandpass show numerous localized brightenings occurring in the EFR. Ephemeral UV bright points, observed in the EFR, are the transition-region counterpart of EBs (see the discussion in Section 2). As noted in the Introduction (Section 1), the formation mechanism of EBs most likely involves chromospheric magnetic reconnection taking place at a BP. 2D and 2.5D models of reconnection at a BP frequently assume that reconnection is due to the formation of a vertical current sheet induced by the pinching of the U-shaped segment of the separatrices, above the BP (Georgoulis et al. 2002; Isobe et al. 2007; Archontis et al. 2009).

However, the present work shows that, as suggested by Billingham et al. (1993), current develops all along the separatrix surfaces (see Figure 5, bottom panels). This implies that reconnection can occur not only at the BP itself, but at different locations on the separatrices. This can explain the fact that EBs can be observed not only at the BP itself but also at the foot-point of the separatrices, for example as reported by Pariat et al. (2004).

Nonetheless, we also observe that the more intense currents develop at the BPs: therefore they remain the most likely place to generate resistive reconnection and would explain why most of the EBs are indeed observed to be cospatial with BPs (Pariat et al. 2004). Even then, formation of strong currents around a BP does not necessarily imply pinching. In Figure 5, the vertical cuts “A” and “B” show that intense currents can develop around BPs, along the separatrices, without necessarily being vertical: in the “A” cut, around $x = 22$ Mm and in “B” around $x = 32$ Mm, intense currents are formed along relatively horizontal separatrices.

Pinching is therefore not a necessary plasma motion to trigger EBs. However, this mechanism may sometimes occur as observed in cut “C.” Around $x = 28$ Mm, two vertical current sheets have built up, the right one being the most intense. They correspond to two Ω -shaped lobes of a serpentine field line which seemed to have been pinched against each other. The horizontal distribution of the current (see Figure 3 and the top panel of Figure 5) present a sigmoid-like structure. This type

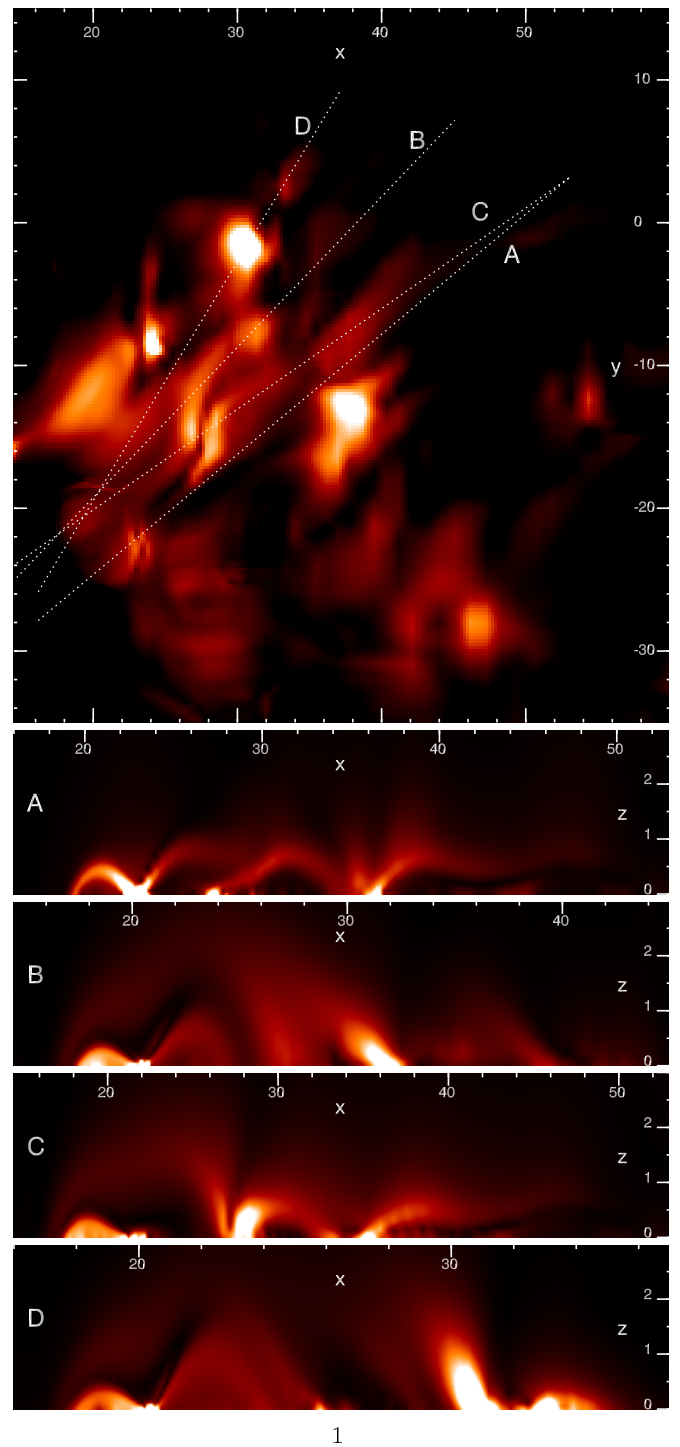


Figure 5. Top panel: distribution of the sum of $|j|/|b|dz$, integrated from $z = 0$ to $z = 3$, in the (x, y) plane with $x \in [15, 60]$ Mm and $y \in [-35, 15]$ Mm at $t = 500$ s. The field of view is the same as in Figures 3 and 4. The intensity is red color-coded with white/light red corresponding to the highest values while black/dark red indicates the absence of currents. The dotted lines correspond to the four vertical 2D cuts of the distribution of $|j|/|b|$ presented in the four bottom panels letter labeled from A to D. The axes labels are in Mm.

of feature is probably typical of the pinching mechanism, as is also observed in the 3D simulation of Archontis et al. (2009).

At $x = 30$ Mm in cut “D,” the current sheet is also nearly vertical. Because of the vertical inclination, this structure appears more vividly in the top panel of Figure 5 (around $(x, y) = (30 \text{ Mm}, -2 \text{ Mm})$). Similarly, in the solar atmosphere

EBs due to a vertical current sheet may be seen preferentially. For a given emitted energy, the intensity of the emission is going to be larger where the current sheet is more vertical since the energy is going to be liberated by reconnection over a more localized domain. This simple argument nonetheless must be modulated by taking into account the full radiative transfer process of the solar chromosphere.

The high cadence UV observations of the EFR also revealed very transient loop-like structures (see Section 2). These very short-lived, dynamic loops can be explained simply by the dissipation of the serpentine current sheets. In the top panel of Figure 5, we note several elongated features with the same direction as the axis of the AR, generally originating from intense localized patches. While these localized patches would correspond to the EBs, the extended structures, which are actually the currents which become concentrated along the serpentine separatrixes, could explain the transient loops observed in the UV images (see Figure 1). In addition, the shape and structure of some examples of these transient loops fit with the interpretation that they correspond to the emerging serpentine field line. Indeed, the peculiar cusp-like shape (λ) of a segment of one of these transient loops (third row of Figure 1) would perfectly correspond to the dipped part of a serpentine separatrix. Because Alfvén velocity is higher at the top of the loop (due to the smaller density), the characteristic timescale of the energy release is smaller at the top of the loop. Therefore the loop structures would be more transient than the EBs.

6. CONCLUSION AND DISCUSSION

The present paper extends our work on the formation and development of a quasi-circular ribbon during a C-class flare that occurred on 2002 November 16 within the AR 10191 (MPAS09). We used the same numerical simulation presented in MPAS09 to study the pre-flare activity taking place in an EFR located in the middle of the AR.

As discussed in Section 2, *TRACE* observations in the 1600 Å bandpass show numerous localized brightenings occurring in the EFR. Their lifetimes and the positions relative to the distribution of the magnetic field allow us to argue that these UV bright points are the photospheric counterpart of EBs. In addition, we also describe for the first time the appearance of numerous very transient loop-like structures. These UV loop transients seem to be related to the EBs: they appear in the EFR, frequently originate from the EBs, and sometimes seem to connect several EBs.

In the present study we used the numerical simulation described in MPAS09 (Section 3) to study the development of the current sheets that may lead to the magnetic reconnections involved in EB formations. We demonstrate that numerous bald patches (BPs) are present at the photospheric level (Section 4.1). We observe that several groups of BPs may be connected by a singular separatrix surface, which assumes a serpentine shape (Section 4.2). The present study does not address the formation of these serpentine field lines, which are most probably the consequence of convection under the solar surface (as simulated by Cheung et al. 2008).

Our study of the 3D distribution of the currents in EFR confirms that current sheets preferentially develop all along these serpentine separatrix surfaces (Section 4.3). Even though we cannot compare directly the locations of these modeled current sheets with those of the UV bright points observed by *TRACE* within the emerging flux area (because of our

oversimplified treatment of this region in our simulation), our result explains why EBs are not necessarily cospatial with BPs but can appear at some other location along BP separatrixes (Section 5). The pinching mechanism, which is frequently assumed for EBs formation, and which essentially derives from 2D models of reconnection, is not necessary to explain EBs. Photospheric shearing motions along BP separatrixes can be an efficient way to build up 3D serpentine intense current sheets and lead to 3D magnetic reconnections that would form EBs. Finally, based on our results, we argue that the serpentine current sheets can simply explain the very transient loops that we have observed in the EFR associated with the EBs.

Overall, our results fit extremely well with the so-called resistive flux emergence model (Pariat et al. 2004; Schmieder & Pariat 2007). In this model, EFRs contain magnetic field lines/surfaces with a serpentine shape around the photospheric layer. Through the BPs that form in the line-tied photosphere during the emergence of these flux tubes, current sheets develop and magnetic reconnection occurs, as manifested in observations as EBs. Successive reconnections allow the dense plasma that is trapped within the BPs to disperse, thus permitting the gradual rise of the magnetic flux from the convection zone to the corona through the photosphere.

It is important to consider that these results have been obtained in the frame of line-tied low- β numerical simulations. Our simulation does not include any real flux emergence (net injection of magnetic flux) and is limited in its ability to fully describe the precise mechanisms of reconnections and radiative transfer which take place in the solar chromosphere. However, we are confident that the fundamental properties of the evolving electric currents are properly modeled by the present simulation. Differential shearing motions on each side of a separatrix have been known to be an efficient way to intensify electric currents along the separatrix (Low & Wolfson 1988; Billingham et al. 1993). The key elements for the current intensification along the separatrix are the line tying and the fact that motions at the different anchorage points of the serpentine separatrixes (BPs and footpoints) are relatively uncorrelated.

Uncorrelated footpoint motions shear differentially the magnetic field lines in each connectivity domain, hence creating magnetic gradients along the separatrixes as well as vorticity which will ensure current buildup and efficient reconnection. The undulation scale of a typical serpentine field line is larger than a few Mm, equal or larger than the typical size of a convection cell. The serpentine field lines spanning several convection cells (Cheung et al. 2008) therefore ensure that uncorrelated motions may be applied at their different footpoints.

Because this work relies on the line-tied approximation, it is subject to the validity of this approximation (Grappin et al. 2008). Line tying assumes that the strong gradients of the thermodynamic quantities at the photosphere/chromosphere are infinitely large. However, these finite gradients may modify the dynamic and the properties of the current sheets which form in these solar layers and, in particular, around the BPs. Karpen et al. (1990, 1991) argued that the dipped part of the field lines would rise due to the effect of the curvature term in the Lorentz force. In addition, they note that electric currents in a non-line-tied atmosphere will have a width of the order of the local pressure scale height and therefore may not be thin enough to explain impulsive fast reconnection and large energy release (Karpen et al. 1990).

However, without a strict line-tying, BP separatrixes intrinsically become quasi-separatrix layers (Longcope 2005) which

nevertheless remain preferential sites for the buildup of intense electric current sheets (e.g., Demoulin et al. 1996; Aulanier et al. 2005b) and for the triggering of magnetic reconnection (Aulanier et al. 2006). The problem is thus whether enough energy can be stored in the current sheets along the serpentine field line with a weak line-tying and whether the dissipation of this current sheets can explain the observational properties of EBs and transient loops. Because an EB is a phenomenon whose total energy is estimated to be in the range $[10^{20}, 10^{21}]$ J (Georgoulis et al. 2002), important energy storage and dissipation are much less stringent for EBs, which frequently occurs in EFR, than for flares.

Regarding the possible rise of the dipped part of the field lines, Delannée & Aulanier (1999) pointed that with typical photospheric values, the curvature radius of the field would have to be smaller than a few hundreds of meters in the photosphere for the uplift force to be efficient. This value, much smaller than the typical curvature of the serpentine field line (both observed or presently simulated), ensures that thin and intense current sheets can develop along the serpentine field lines. In addition, in serpentine field lines, plasma tends to flow toward the bottom of the dipped structure (Fan 2001; Magara & Longcope 2003), increasing the plasma density and enhancing the line tying. Finally, Cheung et al. (2008) showed that the U-shaped section of the field lines could eventually retract within the solar convection zone driven by convective downflows. The convective motion would there even further enforce the line tying. Let us note that simultaneously they would also lead to a pinching of the branch of the U-loop that would result in an (apparent) flux cancellation and in magnetic reconnection that would be observed as an EB.

The results of this simulation must, therefore, be compared with numerical simulation that fully includes a stratified atmosphere, from the upper convection zone to the corona and eventually some radiative transfer model (e.g., Abbett 2007; Martínez-Sykora et al. 2008). However, the question that really matters regarding the formation of EBs and the rise of emerging flux tubes is more related to the dynamics of photospheric/chromospheric reconnection which is poorly understood at present. The present study shows that 3D thin currents develop along the topological structures as well as in more 2D pinching-like structures. Both can lead to magnetic reconnection and account for the diversity of the observed features that can be found in emerging active regions: UV bright points, EBs, and also the transient loops reported in the present study. However, the detailed physics of the reconnection mechanism determines which intensified current sheet will effectively release energy. Studies of reconnection in the lower layer of the solar atmosphere (e.g., Zweibel 1989; Ji & Song 2001; Leake & Arber 2006; Litvinenko & Chae 2009), where the plasma β is close to 1 and the ionization fraction is low, will help to determine the precise process of magnetic flux emergence by multiple magnetic reconnections.

E.P. is indebted to J. Karpen for her thorough reading of this manuscript and pertinent comments that improved the discussion. E.P. also thanks V. Archontis, the organizers, and the fellow participants of the Flux Emergence Workshop 2008 in Kyoto for stimulating discussions. Our MHD calculations were done on the dual-core quadri-Opteron computers of the Service Informatique de l'Observatoire de Paris (SIO). The work of E.P. was supported, in part, by the NASA HTP, LWS TR&T, and SR&T programs. The work of S.M. is funded by a fellowship of Délégation Générale pour l'Armement (DGA).

Financial support by the European Commission through the SOLAIRE Network (MTRN-CT-2006-035484) is gratefully acknowledged.

REFERENCES

- Abbett, W. P. 2007, *ApJ*, **665**, 1469
- Arber, T. D., Haynes, M., & Leake, J. E. 2007, *ApJ*, **666**, 541
- Archontis, V. 2008, *J. Geophys. Res. (Space Phys.)*, **113**, 3
- Archontis, V., Hood, A. W., Savcheva, A., Golub, L., & Deluca, E. 2009, *ApJ*, **691**, 1276
- Archontis, V., Moreno-Insertis, F., Galsgaard, K., Hood, A., & O'Shea, E. 2004, *A&A*, **426**, 1047
- Aulanier, G., Démoulin, P., & Grappin, R. 2005a, *A&A*, **430**, 1067
- Aulanier, G., Démoulin, P., Schmieder, B., Fang, C., & Tang, Y. H. 1998, *Sol. Phys.*, **183**, 369
- Aulanier, G., Pariat, E., & Démoulin, P. 2005b, *A&A*, **444**, 961
- Aulanier, G., Pariat, E., Démoulin, P., & Devore, C. R. 2006, *Sol. Phys.*, **238**, 347
- Bernasconi, P. N., Rust, D. M., Eaton, H. A., & Murphy, G. A. 2000, *BAAS*, **32**, 826
- Bernasconi, P. N., Rust, D. M., Georgoulis, M. K., & Labonte, B. J. 2002, *Sol. Phys.*, **209**, 119
- Billinghurst, M. N., Craig, I. J. D., & Sneyd, A. D. 1993, *A&A*, **279**, 589
- Cheung, M. C. M., Schüssler, M., & Moreno-Insertis, F. 2007, *A&A*, **467**, 703
- Cheung, M. C. M., Schüssler, M., Tarbell, T. D., & Title, A. M. 2008, *ApJ*, **687**, 1373
- Delannée, C., & Aulanier, G. 1999, *Sol. Phys.*, **190**, 107
- Demoulin, P., Henoux, J. C., Priest, E. R., & Mandrini, C. H. 1996, *A&A*, **308**, 643
- DeRosa, M. L., et al. 2009, *ApJ*, **696**, 1780
- Ellerman, F. 1917, *ApJ*, **46**, 298
- Fan, Y. 2001, *ApJ*, **554**, L111
- Fang, C., Tang, Y. H., Xu, Z., Ding, M. D., & Chen, P. F. 2006, *ApJ*, **643**, 1325
- Galsgaard, K., Archontis, V., Moreno-Insertis, F., & Hood, A. W. 2007, *ApJ*, **666**, 516
- Georgoulis, M. K., Rust, D. M., Bernasconi, P. N., & Schmieder, B. 2002, *ApJ*, **575**, 506
- Grappin, R., Aulanier, G., & Pinto, R. 2008, *A&A*, **490**, 353
- Handy, B. N., et al. 1999, *Sol. Phys.*, **187**, 229
- Heyvaerts, J., Priest, E. R., & Rust, D. M. 1977, *ApJ*, **216**, 123
- Isobe, H., Miyagoshi, T., Shibata, K., & Yokoyama, T. 2005, *Nature*, **434**, 478
- Isobe, H., Tripathi, D., & Archontis, V. 2007, *ApJ*, **657**, L53
- Ji, H. S., & Song, M. T. 2001, *ApJ*, **556**, 1017
- Karpen, J. T., Antiochos, S. K., & Devore, C. R. 1990, *ApJ*, **356**, L67
- Karpen, J. T., Antiochos, S. K., & Devore, C. R. 1991, *ApJ*, **382**, 327
- Kitai, R. 1983, *Sol. Phys.*, **87**, 135
- Leake, J. E., & Arber, T. D. 2006, *A&A*, **450**, 805
- Litvinenko, Y. E., & Chae, J. 2009, *A&A*, **495**, 953
- Longcope, D. W. 2005, *Living Rev. Sol. Phys.*, **2**, 7
- Low, B. C., & Wolfson, R. 1988, *ApJ*, **324**, 574
- Magara, T. 2001, *ApJ*, **549**, 608
- Magara, T. 2008, *ApJ*, **685**, L91
- Magara, T., & Longcope, D. W. 2003, *ApJ*, **586**, 630
- Mandrini, C. H., Démoulin, P., Schmieder, B., Deng, Y. Y., & Rudawy, P. 2002, *A&A*, **391**, 317
- Martínez-Sykora, J., Hansteen, V., & Carlsson, M. 2008, *ApJ*, **679**, 871
- Masson, S., Pariat, E., Aulanier, A., & Schrijver, C. 2009, *ApJ*, **700**, 559 (MPAS09)
- Metcalf, T. R., Jiao, L., McClymont, A. N., Canfield, R. C., & Uitenbroek, H. 1995, *ApJ*, **439**, 474
- Metcalf, T. R., et al. 2008, *Sol. Phys.*, **247**, 269
- Moreno-Insertis, F. 2007, in ASP Conf. Ser. 369, *New Solar Physics with Solar-B Mission*, ed. K. Shibata, S. Nagata, & T. Sakurai (San Francisco, CA: ASP), 335
- Murray, M. J., & Hood, A. W. 2008, *A&A*, **479**, 567
- Murray, M. J., Hood, A. W., Moreno-Insertis, F., Galsgaard, K., & Archontis, V. 2006, *A&A*, **460**, 909
- Okamoto, T. J., et al. 2008, *ApJ*, **673**, L215
- Otsuji, K., et al. 2007, *PASJ*, **59**, 649
- Pariat, E., Aulanier, G., Schmieder, B., Georgoulis, M. K., Rust, D. M., & Bernasconi, P. N. 2004, *ApJ*, **614**, 1099
- Pariat, E., Aulanier, G., Schmieder, B., Georgoulis, M. K., Rust, D. M., & Bernasconi, P. N. 2006, *Adv. Space Res.*, **38**, 902

- Pariat, E., Schmieder, B., Berlicki, A., Deng, Y., Mein, N., López Ariste, A., & Wang, S. 2007, *A&A*, **473**, 279
- Parker, E. N. 1966, *ApJ*, **145**, 811
- Qiu, J., Ding, M. D., Wang, H., Denker, C., & Goode, P. R. 2000, *ApJ*, **544**, L157
- Rust, D. M., & Keil, S. L. 1992, *Sol. Phys.*, **140**, 55
- Scherrer, P. H., et al. 1995, *Sol. Phys.*, **162**, 129
- Schmieder, B., & Pariat, E. 2007, *Scholarpedia*, **2**, 4335
- Schrijver, C. J., et al. 2008, *ApJ*, **675**, 1637
- Schrijver, C. J., DeRosa, M. L., Title, A. M., & Metcalf, T. R. 2005, *ApJ*, **628**, 501
- Severny, A. B. 1968, in *Mass Motions in Solar Flares and Related Phenomena*, ed. Y. Oehman (Stockholm: Almqvist & Wiksell), 71
- Strous, L. H., Scharmer, G., Tarbell, T. D., Title, A. M., & Zwaan, C. 1996, *A&A*, **306**, 947
- Titov, V. S., & Démoulin, P. 1999, *A&A*, **351**, 707
- Titov, V. S., Priest, E. R., & Demoulin, P. 1993, *A&A*, **276**, 564
- Tsuneta, S., et al. 2008, *Sol. Phys.*, **249**, 167
- Vekstein, G., Priest, E. R., & Amari, T. 1991, *A&A*, **243**, 492
- Watanabe, H., et al. 2008, *ApJ*, **684**, 736
- Zwaan, C. 1985, *Sol. Phys.*, **100**, 397
- Zweibel, E. G. 1989, *ApJ*, **340**, 550